

Entrainment and horizontal atmospheric transport of microplastics from soil

Chemosphere

Abbasi, Sajjad; Rezaei, Mahrooz; Mina, Monireh; Sameni, Abdolmajid; Oleszczuk, Patryk et al

<https://doi.org/10.1016/j.chemosphere.2023.138150>

This publication is made publicly available in the institutional repository of Wageningen University and Research, under the terms of article 25fa of the Dutch Copyright Act, also known as the Amendment Taverne.

Article 25fa states that the author of a short scientific work funded either wholly or partially by Dutch public funds is entitled to make that work publicly available for no consideration following a reasonable period of time after the work was first published, provided that clear reference is made to the source of the first publication of the work.

This publication is distributed using the principles as determined in the Association of Universities in the Netherlands (VSNU) 'Article 25fa implementation' project. According to these principles research outputs of researchers employed by Dutch Universities that comply with the legal requirements of Article 25fa of the Dutch Copyright Act are distributed online and free of cost or other barriers in institutional repositories. Research outputs are distributed six months after their first online publication in the original published version and with proper attribution to the source of the original publication.

You are permitted to download and use the publication for personal purposes. All rights remain with the author(s) and / or copyright owner(s) of this work. Any use of the publication or parts of it other than authorised under article 25fa of the Dutch Copyright act is prohibited. Wageningen University & Research and the author(s) of this publication shall not be held responsible or liable for any damages resulting from your (re)use of this publication.

For questions regarding the public availability of this publication please contact
openaccess.library@wur.nl



Entrainment and horizontal atmospheric transport of microplastics from soil



Sajjad Abbasi ^{a,b,g,*}, Mahrooz Rezaei ^{c,1}, Monireh Mina ^d, Abdolmajid Sameni ^d, Patryk Oleszczuk ^g, Andrew Turner ^e, Coen Ritsema ^f

^a Department of Earth Sciences, College of Science, Shiraz University, Shiraz 71454, Iran

^b Centre for Environmental Studies and Emerging Pollutants (ZISTANO), Shiraz University, Shiraz, Iran

^c Meteorology and Air Quality Group, Wageningen University & Research, P.O. Box 47, 6700, AA Wageningen, the Netherlands

^d Department of Soil Science, School of Agriculture, Shiraz University, Shiraz, Iran

^e School of Geography, Earth and Environmental Sciences, University of Plymouth, PL4 8AA, UK

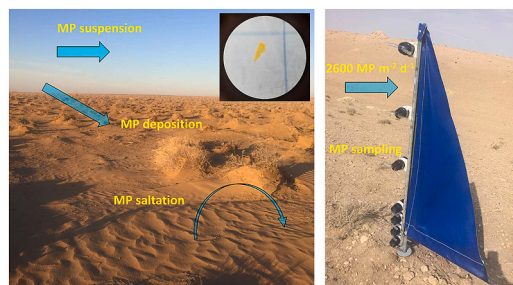
^f Soil Physics and Land Management Group, Wageningen University & Research, P.O. Box 47, 6700 AA Wageningen, the Netherlands

^g Department of Radiochemistry and Environment Chemistry, Faculty of Chemistry, Maria Curie-Skłodowska University, 20-031, Lublin, Poland

HIGHLIGHTS

- Horizontal sediment traps have collected microplastics (MPs) from an arid region.
- Number of MPs (0–21) was variable between sites and at different heights (up to 1 m).
- Most MPs were <250 µm fibres of polyethylene, nylon and polypropylene.
- Median vertically-averaged horizontal flux was about 2630 MP m⁻² d⁻¹.
- Observations attributed to mixing of background airborne MPs with MPs suspended from soil.

GRAPHICAL ABSTRACT



ARTICLE INFO

Handling Editor: Tida Ge

Keywords:

Soils
Wind erosion
Entrainment
Transport
Saltation
MWAC Sampler

ABSTRACT

Soils are an important source of microplastics (MPs) to the atmosphere but the fluxes and mechanisms involved in MPs entrainment are not well understood. In the present study, a series of horizontally aligned sediment traps have been deployed at different heights within 1 m above the ground for a two-month period at various locations in an arid region (Sarakhs, Iran). MPs were isolated from sediments and were quantified and characterised according to size, colour, shape and polymer composition by established techniques. Most MPs were <250 µm in length, fibres were the most important shape, black and blue-green were the dominant colours, and polymer abundance decreased in the order polyethylene > nylon > polypropylene > polystyrene > polyethylene terephthalate. The distributions of sediment mass (range <0.01–9 g) and number of MPs (range = 0 to 21) were heterogeneous, both between sites and at the different heights sampled, and yielded median, vertically-averaged horizontal fluxes for the region of about 450 g m⁻² d⁻¹ and 2600 MP m⁻² d⁻¹, respectively. However, when data were pooled, the number of MPs normalised to sediment mass exhibited a significant inverse relationship with sediment mass, an effect attributed to the presence of ambient suspended MPs and sediment that are diluted by the suspension of soil and deposited MPs at higher wind speeds. The mechanisms of MP saltation and

* Corresponding author. Department of Earth Sciences, College of Science, Shiraz University, Shiraz 71454, Iran.

E-mail addresses: sajjad.abbasi@shirazu.ac.ir, sajjad.abbasi.h@gmail.com (S. Abbasi).

¹ These authors contributed equally.

entrainment were not ascertained but a theoretical framework for threshold shear velocity based on regularly-shaped particles and density considerations is presented. Further experimental work is required to verify this framework, and in particular for fibrous MPs with different aerodynamic properties to soil particles.

1. Introduction

Although the recent literature has identified the atmosphere as a key environmental compartment for microplastics (MPs) (Wang et al., 2021; Ding et al., 2022; Evangelou et al., 2022), little is understood about the processes controlling their inputs, transport and fate in this setting. Processes acting on MPs are likely the same as those acting on geosolids, like soils, sediments and dusts, and include saltation, entrainment, advection, horizontal conveyance, long-range transport and deposition (Kallenbach et al., 2022). However, MPs have very different properties to geosolids, with lower densities and different aspect ratios (especially for films and fibres), and consequently, different inter-particle forces and aerodynamic characteristics (Ravi et al., 2020).

Several studies have used passive sampling devices to collect, quantify and characterise MPs that have undergone dry and/or wet deposition (Cai et al., 2017; Klein and Fischer, 2019; Abbasi and Turner, 2021; Xiong et al., 2022) and have concluded that the atmosphere is instrumental to their long-range transport. Far less understood, however, is how MPs are initially entrained into the atmosphere from the terrestrial environment during wind-erosion and how MPs are subsequently transported horizontally. Empirical studies in wind tunnels deployed in the field (Rezaei et al., 2019, 2022) or in the laboratory (Bullard et al., 2021) demonstrate clear enrichment of MPs in suspended material compared with underlying soils but threshold speeds for MP suspension and horizontal MP fluxes have not been determined.

The modified Wilson and Cooke (MWAC) sediment catcher (Wilson and Cooke, 1980; Kuntze et al., 1990) consists of a vertical array of traps that allows the horizontal (including saltation) sediment mass flux to be measured and horizontal mass transport to be calculated. Accordingly, the MWAC is commonly employed in field studies of aeolian transport and wind erosion over arid and semi-arid soils (Mendez et al., 2011;

Sterk et al., 2012; Webb et al., 2016). In the present study, a series of customized, 1-m modified MWAC sediment catchers has been deployed for an extended (two-month) period in an arid region subject to significant wind-erosion to capture both sediment and MPs at different heights above the ground, with MPs subsequently isolated and characterised by established methods. The spatial and vertical distributions of MPs and eroded sediments have been examined in order to better understand the nature and mechanisms of MPs entrainment and horizontal transport over soils susceptible to erosion and to explore any relationships between processes and effects acting on MPs and soils.

2. Material and methods

2.1. Study area

The location of Sarakhs is shown in Fig. 1 along with the precise sites where sampling was undertaken. Sarakhs is a 2000 km² sub-basin of the Qarakhm Basin in north-east Iran that is bound to the west and southwest by the Bazangan and Shurluq mountains and to the north and east by the border with Turkmenistan (with the eastern border defined by the Harirud River). The majority of Sarakhs consists of a plain at 300–500 m above sea level that is subject to desertification because of an arid climate, low precipitation (annual average precipitation ~ 185 mm), unfavourable soil, land use changes, alluvial aquifer exploitation and wind erosion (Koohbanani et al., 2018; Sarbazi et al., 2020). Erosive conditions are intensified between late May and late September because of strong, persistent north-westerly to north-easterly winds (the “120-day wind”) that are channelled into the region by the surrounding topography (Alizadeh-Chobari et al., 2014).

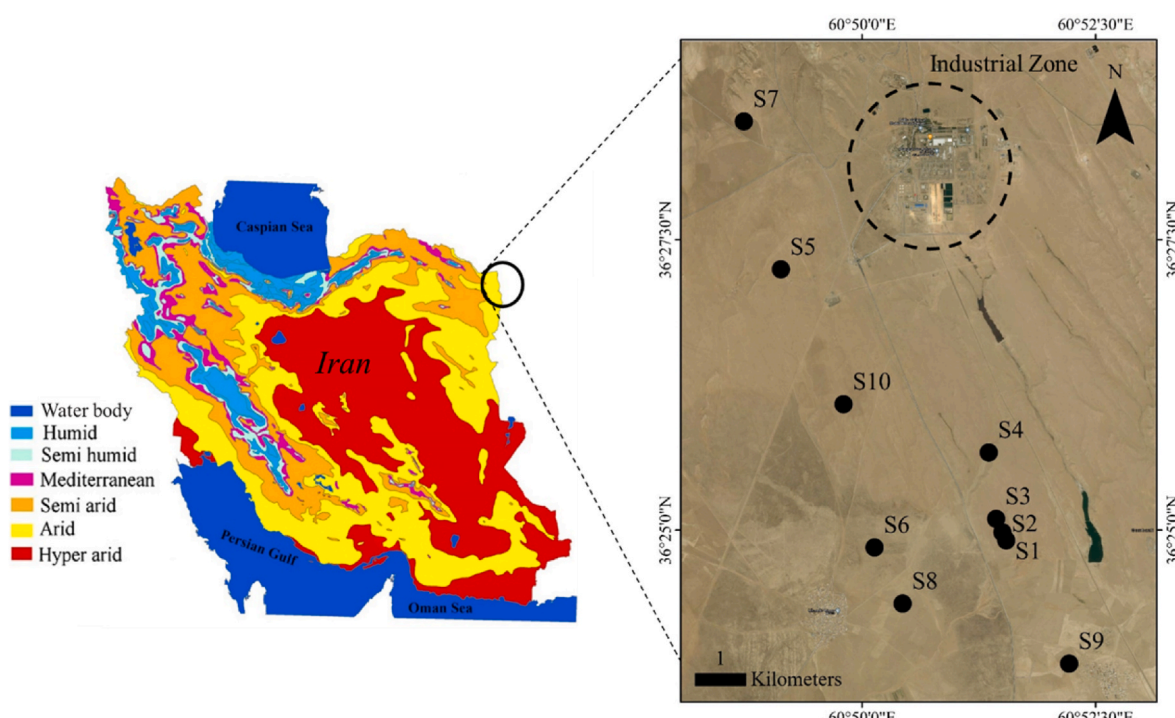


Fig. 1. Location of Sarakhs and the ten sites selected for study.

2.2. Sample collection

Airborne sediment and MPs were sampled using a series of MWAC sediment catchers deployed at ten sites in central Sarakhs (Fig. 1) from July 17, 2019 to September 12, 2019 (a period of 57 days). Sampling sites included those within 5 km of an industrial zone housing oil and gas refining (S5 and S7) and those remote from any human influence (e.g., S6, S8 and S9). A wind rose defining the frequencies of wind speed and direction at a height of 10 m in Sarakhs during the study period is shown in Fig. 2. Winds were predominantly northerly to north-westerly, with a maximum speed above 11 m s^{-1} , an overall average speed of about 2 m s^{-1} and calm conditions for about 30% of the time. Gravimetric analysis of 50, ~50 g surface soils sampled throughout the region studied and that had been mechanically fractionated through a series of stainless steel sieves as part of a parallel research project revealed the following approximate grain size distributions (mean \pm one standard deviation and as percentages): $>4 \text{ mm} = 5.9 \pm 3.9$; $2-4 \text{ mm} = 10.2 \pm 6.5$; $1-2 \text{ mm} = 9.3 \pm 4.2$; $0.2-1 \text{ mm} = 20.1 \pm 6.3$; $0.05-0.2 \text{ mm} = 49.4 \pm 14.3$; $<0.05 \text{ mm} = 5.2 \pm 2.2$.

Each MWAC sediment catcher consisted of a vertical array of seven sediment traps at heights above the ground recommended by Sterk and Raats (1996): namely, 0.05, 0.12, 0.19, 0.26, 0.50, 0.75 and 1.00 m. Traps were 100-mL amber glass bottles with 8-mm diameter glass inlet and outlet tubes that were orientated horizontally on a 1.5 m central mast. The mast was fitted with a vane that allowed the inlet tubes to face the wind, with air-borne particles that enter through the inlet tubes settling in the traps as air slows down and subsequently escapes through the outlets. MWAC sediment catchers were secured by inserting the lower 40 cm of the central pole into a metal tube that had been buried in the soil. The surrounding soil was smoothed with a metal trowel and sediment catchers were left for a period of two weeks in order to allow the disturbed terrain to acclimatise before bottles were cleaned with filtered water and dried and sampling began.

2.3. Microplastic extraction

At the end of the sampling period, bottles were wrapped in aluminium foil and transported to the laboratory. Samples were carefully transferred to pre-weighed 600-mL beakers using a stainless steel spoon and weighed on an electronic balance (Libron AEL-40SM, Shimadzu, Japan) before being sieved through a 5-mm stainless steel mesh. Each sieved sample (up to 10 g) was then weighed into a clean beaker to which 30 mL of 30% H_2O_2 (Arman Sina, Tehran) was added, with oxidation proceeding at room temperature until bubble formation ceased. Remaining particulate matter was washed with filtered, deionised water through a 150 mm diameter S&S filter paper (blue band, grade 589/3, 2 μm pore size) housed in a glass-ceramic vacuum filtration kit before being placed on an aluminium tray, covered with foil and dried in a sand bath at 60°C for 2 h.

MPs were isolated according to Abbasi et al. (2019). Briefly, dried, digested samples were transferred to 300-mL solutions of saturated ZnCl_2 (Arman Sina, Tehran; density $1.6-1.8 \text{ g cm}^{-3}$) in a series of clean glass beakers, and the decanted contents were subsequently centrifuged at 4000 rpm before supernatants were vacuum-filtered through S&S filter papers. Suspension, decanting and centrifugation were repeated twice before resulting filters were air-dried for 48 h at 25°C in a metal cabinet and transferred to glass Petri dishes for physical and chemical characterisation.

2.4. Microplastic identification and characterisation

MPs on filters were identified and quantified under a binocular microscope (Carl-Zeiss) at 40 x to 200 x magnification and with the aid of ImageJ software. Identification was based on thickness and cross sectional properties, shininess, hardness, surface structure and reaction to a hot, 250 μm -diameter, stainless steel needle. Particle size, with a lower limit of about 20–50 μm depending on shape and colour, was

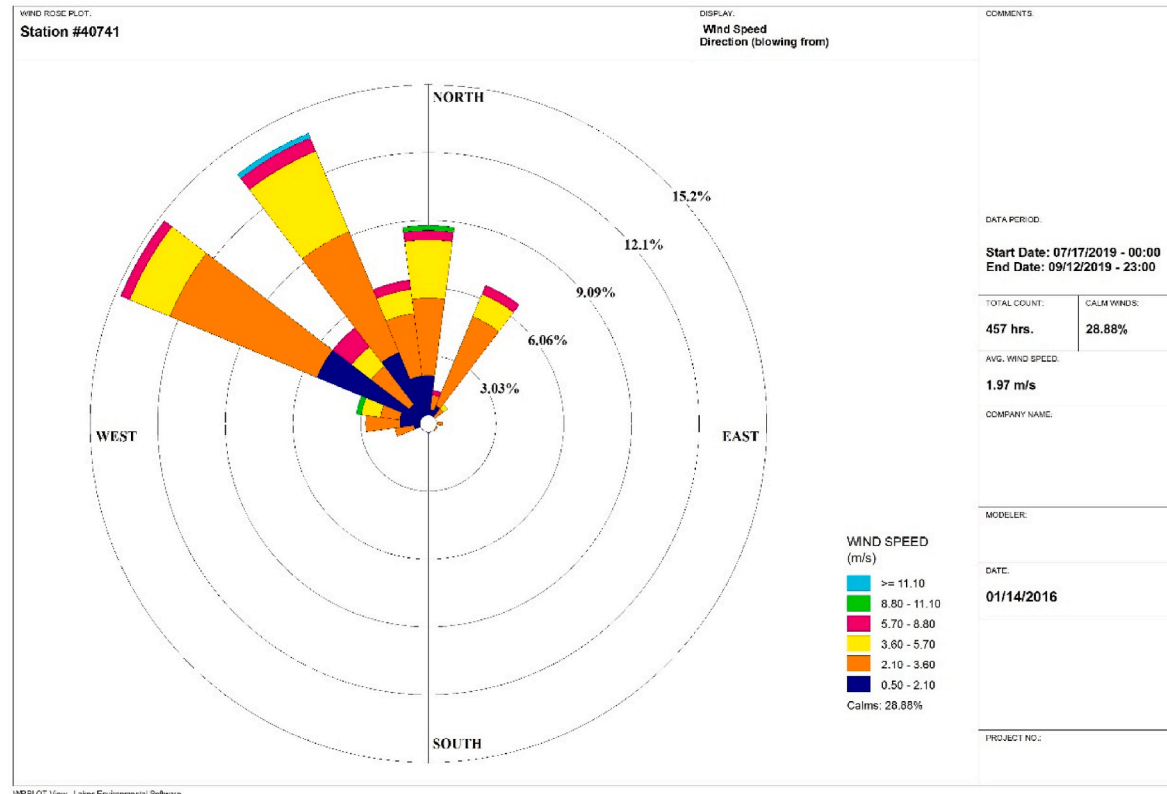


Fig. 2. A wind rose for Sarakhs at a height of 10 m during the period of study.

estimated along the length of the longest axis, L ($L \leq 100 \mu\text{m}$, $100 < L \leq 250 \mu\text{m}$, $250 < L \leq 500 \mu\text{m}$, $500 < L \leq 1000 \mu\text{m}$, $L > 1000 \mu\text{m}$), and colour was grouped as black-grey, yellow-orange, white-transparent, red-pink or blue-green. Shape was classified as film, fragment, spherule-granule or fibre, with the latter defined as having a length to diameter ratio of at least three.

The polymeric composition of all MPs isolated from sites S3 and S9 (that is, at all heights at two sites where MPs were relatively abundant; $n = 88$) and an additional random 19 MPs from other sites was determined using a micro-Raman spectrometer (LabRAM HR, Horiba, Japan) with a laser of 785 nm, a Raman shift of 400–1800 cm^{-1} and acquisition times between 20 and 30 s. Surface morphology was examined on MPs from sites S3 and S9, after they had been mounted on microscope slides and gold-coated, using a high vacuum scanning electron microscope (SEM; TESCAN Vega 3, Czech Republic) operated at 20 kV and with a resolution of 2 nm.

2.5. X-ray diffraction analysis

Sieved samples from every bottle at sites S3 and S9 were subject to X-ray diffraction (XRD) analysis. Data were collected using a Bruker-D8 ADVANCE diffractometer operated in reflection geometry at 40 kV and 30 mA and with a Cu-K α source. The 20 scan ranged from 5° to 70°, with a step size of 0.02° and a counting time of 1 s, and phase identifications were conducted using the X-powder software (version 2010.01.45 PRO; Martin-Islán, Granada, Spain) supported by the Powder Diffraction File-2 database of the International Centre for Diffraction Data. Quantitative X-ray diffraction analysis was performed with PROFEX software (version 3.10.2; Döbelin and Kleeberg, Bettlach, Switzerland) and the Rietveld refinement kernel, BGGMN (version 4.2.22, Netherlands Energy Research Foundation ECN, Rietveld, Petten, The Netherlands). To evaluate the reliability of the quantitative results, the weighted-profile factor, expected R-factor and goodness of fit factor were monitored.

2.6. Quality assurance and quality control

All reagents and distilled water were filtered through S&S blue band filters and kept in glass containers to prevent plastic and fibre contamination during sample processing. Operators wore white cotton laboratory coats and samples and containers were protected by aluminium foil where possible. Work surfaces were thoroughly cleaned with ethanol, glassware was cleaned with distilled water, and all windows and doors were kept closed. Analysis of five blank filters, derived from the processing of filtered water in glass bowls exposed to the same conditions as the samples, revealed no MP contamination.

As positive controls, ten polyethylene particles and ten polyvinyl chloride particles (both white and spherical and between 20 and 250 μm

in diameter) were added to three glass beakers containing 500 mL of distilled water. Following digestion, isolation and identification as above, all added MPs were recovered.

2.7. Data processing and statistics

Data analysis and statistical tests were performed in Minitab v19. Departures from normality were identified using the Anderson-Darling test ($p > 0.95$ for normality). Non-normal data was summarised in terms of the median and lower and upper quartiles, and differences in median values were detected using a series of Kruskal-Wallis tests ($\alpha = 0.05$). Linear regressions and model calculations were performed in Excel (2013).

3. Results

The dry masses of sediment captured by the traps at each site in the Sarakhs region are shown in Table 1, along with statistical summaries based on non-normal distributions. Masses range from $<1 \text{ mg}$ to about 9 g, and there were significant differences in median masses ($p < 0.001$) between sites. Because of the inter-site variability, however, there were no significant differences ($p > 0.05$) in median masses collected at the different heights above the ground. Moreover, there were no clear height-dependent trends in dry mass at any site, with the maximum and minimum quantities of sediment encountered at various heights amongst the different locations.

XRD analysis of samples at sites S3 and S9 revealed that the principal minerals were quartz (~60–80%), calcite (~5–21%) and albite (~7–22%), with one or more of dolomite, kaolinite and illite present below about 5%. Specific gravities, derived from the mineralogical content, ranged from 2.53 to 2.67 g cm^{-3} (mean = 2.65 g cm^{-3}) but displayed no clear differences between the two sites or with height above the ground.

The number of MPs captured by the traps at each height is shown in Table 2, along with statistical summaries based on non-normal distributions. Overall, 570 MPs were detected, with numbers in individual traps ranging from 0 to 21. There were no significant differences ($p > 0.05$) in median values between either location or height and there were no clear relationships between MP number and height. Fibres dominated MPs by shape (64.0%), with smaller contributions from fragments (26.7%), films (5.8%) and spherules (3.5%). Regarding colour, black or blue-green were most abundant (more than 30% each), with white, red-pink and yellow-orange comprising about 15%, 14% and 5%, respectively. The size distribution of MPs was skewed towards the finer fractions, with about 64% below 100 μm , 34% between 100 and 250 μm and about 2% between 250 and 500 μm ; significantly, no MPs were detected above 500 μm . As with overall MPs abundance, there were no clear shifts in distributions of shape, colour or size between the different sites or as a

Table 1

Dry masses of sediment, in g, collected by the traps at the different heights at each sampling site in the Sarakhs region over a period of 57 days. Median values and lower and upper quartiles are also shown as statistical summaries for each site and each height.

site	height, m						median	Q1	Q3
	1.00	0.75	0.50	0.26	0.19	0.12			
S1	0.49	1.01	0.10	3.75	3.67	3.22	0.92	1.01	0.71
S2	0.09	4.69	0.86	4.16	0.94	0.96	1.04	0.96	0.90
S3	0.04	3.11	1.34	1.78	1.71	0.04	1.19	1.34	0.62
S4	3.67	0.15	0.01	<0.01	0.13	0.13	0.43	0.14	0.13
S5	3.58	2.68	2.94	5.44	5.78	6.89	7.13	5.44	3.26
S6	1.27	4.75	3.21	5.28	0.26	3.02	2.47	3.02	3.98
S7	0.01	0.27	3.51	0.58	2.94	0.80	0.32	0.58	0.30
S8	4.41	4.00	4.93	4.40	4.95	5.36	4.48	4.48	4.41
S9	4.99	5.32	6.96	6.71	4.88	5.44	8.89	5.44	5.16
S10	0.43	0.24	4.99	1.20	3.14	1.26	0.64	1.20	0.54
median	0.88	2.90	3.08	4.16	3.04	2.14	1.12	2.90	1.63
Q1	0.18	0.46	0.98	1.78	1.13	0.84	0.71	0.97	0.56
Q3	3.65	4.52	4.58	5.28	4.58	4.83	3.98	4.12	4.70

Table 2

Number of MPs collected by the traps at the different heights at each sampling site in the Sarakhs region over a period of 57 days. Median values and lower and upper quartiles are also shown as statistical summaries for each site and each height.

site	height, m						median	Q1	Q3
	1.00	0.75	0.50	0.26	0.19	0.12			
S1	9	6	4	5	6	11	10	6.0	5.5
S2	5	4	6	5	8	3	6	5.0	4.5
S3	9	7	5	6	6	2	7	6.0	5.5
S4	2	5	8	0	10	20	11	8.0	3.5
S5	2	7	7	8	16	12	18	8.0	7.0
S6	9	10	4	10	10	13	9	10.0	9.0
S7	5	6	5	7	7	7	16	7.0	5.5
S8	8	8	5	10	5	10	19	8.0	6.5
S9	5	2	14	10	3	6	6	6.0	4.0
S10	11	4	10	10	9	21	20	10.0	9.5
median	6.5	6.0	5.5	7.5	7.5	10.5	10.5	7.5	9.0
Q1	5.0	4.3	5.0	5.3	6.0	6.3	7.5	6.0	4.8
Q3	9.0	7.0	7.8	10.0	9.8	12.8	17.5	8.0	6.9

function of height above the ground.

The number of MPs detected normalised to the quantity of sediment captured is shown for each site and height in Table 3, along with statistical summaries based on non-normal distributions. Values range from 0 to 800 MP g⁻¹ overall, and vary widely both between and within sites, with maximum and minimum values occurring at different heights among the different sites. There were significant differences ($p < 0.05$) in median values between sites but not between different heights.

A summary of the results arising from Raman analysis is shown in Fig. 3. Of 107 samples isolated from sites 3 and 9 and from a selection of other sites and heights, 102 were petroleum-based plastics, one was a natural or synthetic rubber (polyisoprene), one was a mineral-based particle (subsequently neglected) and three returned a match with the additive, polyethylene oxide. More than one-half of the samples were constructed of polyethylene, nylon and polypropylene, and fibres were the most important shape amongst these polymers and poly-phenylsulfone. Fragments were the most abundant shape amongst the remaining polymers and films were observed in MPs constructed of polyethylene, nylon, polystyrene and polyethylene terephthalate while spherules were observed in MPs constructed of polyethylene, nylon and polystyrene. Regarding sites 3 and 9, there was no dependency of MP polymer on height above ground, with both low-density polymers ($< 1 \text{ g cm}^{-3}$; polyethylene and polypropylene) and high-density polymers ($> 1.2 \text{ g cm}^{-3}$; polyvinyl chloride, polyethylene terephthalate, poly-phenylsulfone) distributed throughout the different heights sampled.

4. Discussion

The distributions of sediment mass captured by the MWAC devices in

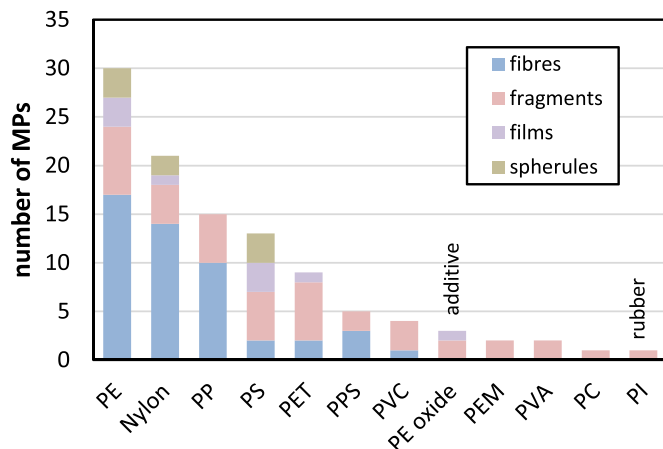


Fig. 3. MPs captured in the Sarakhs region ($n = 106$, and including a rubber and three “additives”) shown in descending order of polymer abundance and classified by shape. PE = polyethylene; PP = polypropylene; PS = polystyrene; PET = polyethylene terephthalate; PPS = polyphenylsulfone; PVC = polyvinyl chloride; PE oxide = poly (ethylene oxide); PEM = poly (ethyl methacrylate); PVA = poly (vinyl alcohol); PC = polycarbonate; PI = polyisoprene.

the Sarakhs region are heterogeneous both between sites and, for a given site, between the different heights sampled. The deployment of MWAC catchers in the short-term or for a single event, for example, is expected to return an exponential, logarithmic or power reduction in sediment mass with increasing height (Dong et al., 2003; Namikas, 2003). In the

Table 3

Number of MPs per g of sediment collected by the traps at the different heights at each sampling site in the Sarakhs region over a period of 57 days. Median values and lower and upper quartiles are also shown as statistical summaries for each site and each height.

site	height, m						median	Q1	Q3
	1.00	0.75	0.50	0.26	0.19	0.12			
S1	18.4	5.9	40.0	1.3	1.6	3.4	10.9	5.9	2.5
S2	55.6	0.9	7.0	1.2	8.5	3.1	5.8	5.8	7.7
S3	225.0	2.3	3.7	3.4	3.5	50.0	5.9	3.7	3.4
S4	0.5	33.3	800.0	0.0	76.9	153.8	25.6	33.3	13.1
S5	0.6	2.6	2.4	1.5	2.8	1.7	2.5	2.4	1.6
S6	7.1	2.1	1.2	1.9	38.5	4.3	3.6	3.6	2.0
S7	500.0	22.2	1.4	12.1	2.4	8.8	50.0	12.1	5.6
S8	1.8	2.0	1.0	2.3	1.0	1.9	4.2	1.9	1.4
S9	1.0	0.4	2.0	1.5	0.6	1.1	0.7	1.0	0.6
S10	25.6	16.7	2.0	8.3	2.9	16.7	31.3	16.7	5.6
median	12.7	2.4	2.2	1.7	2.8	3.9	5.8	2.8	4.8
Q1	1.2	2.0	1.6	1.4	1.8	2.2	3.8	2.7	1.7
Q3	48.1	14.0	6.2	3.1	7.3	14.7	21.9	10.5	5.0

present study, however, we required deployment over an extended period, covering multiple events or processes (e.g., dust storms and streamers) of different intensities and from different wind directions, to capture sufficient material for reliable MPs isolation. MPs sampled by the MWAC sediment catchers are also heterogeneously distributed on a number basis, and both spatially and as a function of height. This heterogeneity encompasses the number of particles and the number normalised to sediment mass, as well as measures of size, colour, shape and polymeric construction.

Because data could not be fitted with regression curves as a function of height, it was not possible to determine vertically integrated horizontal fluxes. However, the net, vertically averaged horizontal fluxes of sediment and MPs within 1 m of the ground in the Sarakhs region may be estimated from the median sediment masses and MP numbers at each site captured through an inlet aperture of 50 mm² and over a deployment period of 57 days. Fluxes, shown in Table 4, range from 49 to 1908 g m⁻² d⁻¹ for sediment, with a median of about 450 g m⁻² d⁻¹, and from 1754 to 3509 MP m⁻² d⁻¹, with a median of about 2600 MP m⁻² d⁻¹. We did not determine vertical, depositional fluxes of sediment or MPs in the present study. However, Abbasi and Turner (2021) measured the monthly dry depositional fluxes of sediment (dust) and MPs over a remote and urbanised region of south-western Iran at a height of a few m above the ground. For the period of July to September, remote and urban mean daily fluxes were about 0.5 and 3 g of sediment m⁻² and 15 and 100 MP m⁻². More widely, depositional rates in both urban and more remote areas are typically on the order of several hundred MP m⁻² d⁻¹ (Cai et al., 2017; Zhou et al., 2017; Allen et al., 2019; Klein and Fischer, 2019). Clearly, therefore, it would appear that the horizontal fluxes of MPs (and sediment) within 1 m of the surface are considerably greater than vertical depositional fluxes.

Despite the spatial and vertical heterogeneity of sediment and MP distributions noted above, when all data are pooled together distinctive relationships between the sediment mass-normalised number of MPs and sediment mass are evident. Fig. 4 shows these relationships for all MPs and for fibrous MPs, along with the corresponding best-fit power-law equations of the form: $y = ax^{-b}$; where a and b are empirical constants. Here, the x-axis might be considered as a scale of the wind-speed or energy available for suspension-resuspension and transport of material. Thus, conditions of low energy are able to readily suspend and transport a relatively high proportion of fine, low density MPs but a low proportion of denser sediment grains, while conditions of high energy are able to suspend and transport greater quantities (and, presumably, sizes) of more local sediment that act to dilute the less variable suspended MP stock. According to the equations of best fit, values defining the respective “ambient” and “diluent” end-members (at sediment masses of 10 mg and 10 g, respectively) are about 660 MP g⁻¹ and 0.74 MP g⁻¹ and 505 MP fibres g⁻¹ and 0.44 MP fibres g⁻¹.

The data obtained in the present study allow us to make some inferences and estimates about the mode of particle transport. Thus, under

Table 4
Vertically averaged (median) horizontal sediment and MP fluxes for the ten sites in the Sarakhs region.

site	sediment, g m ⁻² d ⁻¹	MP m ⁻² d ⁻¹
S1	354	2105
S2	337	1754
S3	470	2105
S4	49	3157
S5	1909	2807
S6	1060	3509
S7	204	2456
S8	1571	2807
S9	1909	2105
S10	421	3509
median	446	2632
Q1	341	2105
Q3	1443	3070

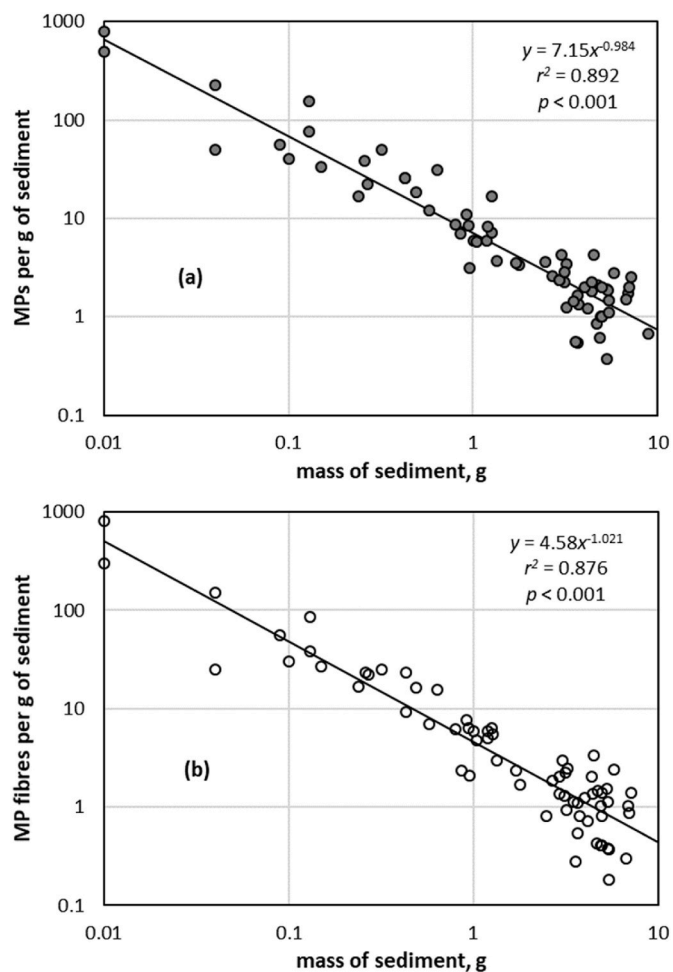


Fig. 4. Numbers of (a) MPs per g of sediment and (b) MP fibres per g of sediment versus mass of sediment for all samples collected in the Sarakhs region.

a typical range of conditions and according to Hudson (1982), sediment particles of density ~ 2.5 g cm⁻³ subject to creep have diameters ranging from 0.5 to 2 mm, those subject to saltation range from 0.05 to 0.5 mm, and those smaller than 0.1 mm are suspended (but without saltation), with overlap arising because of differences in (precise) particle density, wind speed and sediment texture. In addition, particles in the finest category may be suspended in the short-term (20–100 μ m) or long-term (<20 μ m) (Kok et al., 2012). Based on the surface particle size data for Sarakhs reported above (Section 2.2) we predict that, on average, 5–10% of soil could be transported (as sediment) by creep, up to 70% could be transported by saltation and up to 50% could become suspended. The configuration of the MWAC sediment catchers does not allow us to estimate creep but the (variable) mass of material retained by the lowest sediment trap suggests that between <1 and 80% of soil may have been transported by saltation close to the ground (~ 50 mm) while the remaining mass retained suggests that between 20% and >99% may have been transported in suspension.

The relative modes of transport of MPs are very different to those of soil particles. Discrepancies arise because of the lower densities of MPs (~ 0.9 – 1.4 g cm⁻³ for the polymers illustrated in Fig. 3) and consequent lower gravitational pulls, their smaller diameters or lengths (mostly below 200 μ m) and, particularly for thin films and fibres with high aspect ratios, very different aerodynamic properties. Although the precise mechanisms and thresholds for MP emissions from soil are unknown, suggestions have been put forward based on theoretical considerations or observations of other low-density particles.

Shao and Lu (2000) and Ravi et al. (2020) provide a semi-empirical expression for the saltation threshold shear velocity, u_{*t} , based on particle density, ρ_p , and particle diameter, D_p :

$$u_{*t} = A_N \sqrt{\frac{\rho_p - \rho_a}{\rho_a} g D_p + \frac{\gamma}{\rho_a D_p}} \quad (1)$$

where ρ_a is the density of air, g is the acceleration due to gravity, A_N is a dimensionless parameter and γ is a constant that accounts for the strength of inter-particle forces. Fig. 5 shows values of u_{*t} as a function of D_p between 50 μm and 2 mm for particles of density 2.65 g cm^{-3} , the mean value obtained from our XRD analyses of sediments, 0.9 g cm^{-3} , representative of low density polymers observed in Sarakhs like polypropylene, and 1.4 g cm^{-3} representative of higher density polymers observed in the region like PET or PVC. Note that shape is constant amongst the different densities and we used the default values for A_N ($= 0.11$) and γ ($= 2.9 \times 10^{-4} \text{ N m}^{-1}$) reported by Ravi et al. (2020) and an air density of 1.225 kg m^{-3} .

For a given particle density, u_{*t} decreases with decreasing D_p until a point of inflection where inter-particle cohesion becomes increasingly important (the second term on the right-hand side of equation (1)). For a given particle diameter, decreasing ρ_p is accompanied by decreasing u_{*t} but the magnitude of any difference decreases with decreasing particle diameter. This means that the difference between shear forces required to suspend soils and MPs diminishes with decreasing particle size such that below about 50 μm they are similar. In other words, at low wind speeds, small soil particles and MPs of similar diameters can be entrained but at higher wind speeds MPs larger than soil particles are subject to suspension.

The framework above provides a general understanding of the suspension of regularly-shaped MPs based on density considerations. Moreover, it is qualitatively consistent with the observations made in our study (see Fig. 4) and with the enrichment of MPs in eroded sediments compared with soils in wind tunnel experiments or other passive capturing devices deployed over different land-uses (Rezaei et al., 2019, 2022; Tian et al., 2022). However, additional effects may be present when MPs and soil particles co-exist and for MPs that have different shapes and aerodynamic diameters. For instance, Koutnik et al. (2021) argue that, in addition to the direct emission from soil surfaces, entrainment of MPs by wind may also proceed via bombardment of saltating soil particles close to the surface and though the disintegration of large particles or aggregates where plastics may be trapped. By contrast, and because of their lower densities, it is unlikely that saltating MPs have sufficient energy to eject mineral particles. Spherical MPs in

particular are also susceptible to migration and burial in heterogeneous soils through armouring and winnowing effects, providing a means by which microbeads may be retained in this environment (Bullard et al., 2021) and accounting for the relatively low abundance of regularly-shaped MPs captured in the present study.

Fibrous MPs are less like soil particles because of their greater aspect ratios. For instance, the ratio for natural mineral particles is typically around 1.5 (Ginoux, 2003), whereas ratios for fibrous MPs may be in the hundreds (Abbasi et al., 2022). Wind tunnel experiments have revealed that 5-mm polyester fibres are more easily entrained than $\sim 200\text{--}250 \mu\text{m}$ diameter polyethylene beads from soil and sand (Bullard et al., 2021), and once entrained fibres have lower settling velocities because of their higher surface area to volume ratio and opposing fluid drag relative to gravitational pull (Brahney et al., 2020). Fibres are also less susceptible to burial in soils than regularly-shaped MPs like spherules because of their shape and pliability (Bullard et al., 2021).

While it is important to understand the mechanisms behind the emission of MPs from soil, it must be appreciated that this environment represents a secondary MP source that acts to redistribute and, potentially, modify material. Thus, the very presence of MPs in a remote region like Sarakhs, where no plastic-based mulch or fertiliser has been applied, requires the long-range transport of MPs in suspension from various primary sources (Allen et al., 2019; Bergmann et al., 2019; Zhang et al., 2019; Brahney et al., 2020). The wind rose data in Fig. 2 suggest that any primary regional sources of MPs in this study are likely to be located to the north or north-west of Sarakhs.

5. Conclusions

The present study has shown that the near-surface ($<1 \text{ m}$) distributions of airborne sediments and MPs captured by vertical arrays of horizontal traps in an arid region are heterogeneous, both spatially and as a function of height above the ground and, for MPs, with respect to colour, shape and polymeric composition. Consequently, estimated vertically-averaged horizontal fluxes of sediment and MPs are variable, ranging from 49 to $1909 \text{ g m}^{-2} \text{ d}^{-1}$ (median = $446 \text{ g m}^{-2} \text{ d}^{-1}$) and 1754 to $3509 \text{ MP m}^{-2} \text{ d}^{-1}$ (median = $2632 \text{ MP m}^{-2} \text{ d}^{-1}$), respectively. Data pooled from all traps, however, results in a significant inverse relationship between MPs normalised to sediment mass as a function of sediment mass, suggesting that a background elevated in MPs relative to fine sediment is diluted by the entrainment of material containing lower quantities of MPs relative to coarser sediment. While these observations, coupled with theoretical considerations, indicate that MPs are more readily suspended and transported than soil particles, further controlled studies are required to elucidate the precise mechanisms responsible.

Credit author statement

Sajjad Abbasi: Conceptualization, Writing-original draft, Initial Idea, Modelling, Methodology, Investigation, Interpretation, Review and Editing, **Mahrooz Rezaei:** Conceptualization, Sampling, Investigation, Review and Editing, **Monireh Mina:** Sampling, Investigation, Laboratory Work, **Abdolmajid Sameni:** Conceptualization, Review and Editing, **Patryk Oleszczuk:** Investigation, Review and Editing, **Andrew Turner:** Conceptualization, Investigation, Writing-final draft, Modelling, Interpretation, Review and Editing, **Coen Ritsema:** Investigation, Review and Editing.

Declaration of competing interest

The authors declare that they have no known competing financial interests or personal relationships that could have appeared to influence the work reported in this paper.

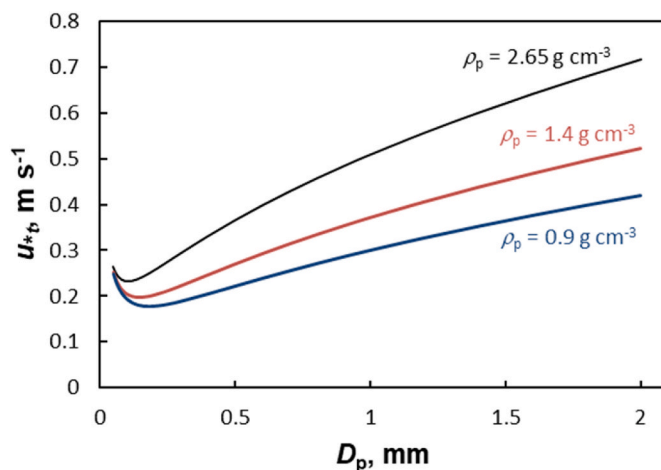


Fig. 5. Saltation threshold shear velocity, u_{*t} , as a function of particle diameter, D_p , for three different particle densities, ρ_p , calculated according to equation (1).

Data availability

Data will be made available on request.

Acknowledgements

We thank Shiraz University for financial and technical support

Appendix A. Supplementary data

Supplementary data to this article can be found online at <https://doi.org/10.1016/j.chemosphere.2023.138150>.

References

Abbasi, S., Keshavarzi, B., Moore, F., Turner, A., Kelly, F.J., Dominguez, A.O., Jaafarzadeh, N., 2019. Distribution and potential health impacts of microplastics and microrubbers in air and street dusts from Asaluyeh County, Iran. *Environ. Pollut.* 244, 153–164.

Abbasi, S., Turner, A., 2021. Dry and wet deposition of microplastics in a semi-arid region (Shiraz, Iran). *Sci. Total Environ.* 786, 147358.

Abbasi, S., Rezaei, M., Ahmadi, F., Turner, A., 2022. Atmospheric transport of microplastics during a dust storm. *Chemosphere* 292, 133456.

Alizadeh-Choobari, O., Zawar-Reza, P., Sturman, A., 2014. The “wind of 120 days” and dust storm activity over the Sistan Basin. *Atmos. Res.* 143, 328–341.

Allen, S., Allen, D., Phoenix, V.R., Le Roux, G., Jimenez, P.D., Simonneau, A., Binet, S., Galop, D., 2019. Atmospheric transport and deposition of microplastics in a remote mountain catchment. *Nat. Geosci.* 12, 339–344.

Bergmann, M., Müttzel, S., Primpke, S., Tekman, M.B., Trachsel, J., Gerdts, G., 2019. White and wonderful? Microplastics prevail in snow from the Alps to the Arctic. *Scientific Advances* 5, eaax1157.

Brahney, J., Hallerud, M., Heim, E., Hahnberger, M., Sukumaran, S., 2020. Plastic rain in protected areas of the United States. *Science* 368, 1257–1260.

Bullard, J.E., Ockelford, A., O'Brien, P., Neuman, C.M., 2021. Preferential transport of microplastics by wind. *Atmos. Environ.* 245, 118038.

Cai, L., Wang, J., Peng, J., Tan, Z., Zhan, Z., Tan, X., Chen, Q., 2017. Characteristic of microplastics in the atmospheric fallout from Dongguan city, China: preliminary research and first evidence. *Environ. Sci. Pollut. Res.* 24, 24928–24935.

Ding, J., Sun, C., He, C., Zheng, L., Dai, D., Li, F., 2022. Atmospheric microplastics in the Northwestern Pacific Ocean: distribution, source, and deposition. *Sci. Total Environ.* 829, 154337.

Dong, Z., Liu, X., Wang, H., Zhao, A., Wang, X., 2003. The flux profile of a blowing sand cloud: a wind tunnel investigation. *Geomorphology* 49, 219–230.

Evangelou, N., Tichy, O., Eckhardt, S., Zwaftink, C.G., Brahney, J., 2022. Sources and fate of atmospheric microplastics revealed from inverse and dispersion modelling: from global emissions to deposition. *J. Hazard Mater.* 432, 128585.

Ginoux, P., 2003. Effects of nonsphericity on mineral dust modelling. *J. Geophys. Res.* 108 (D2), 4052.

Hudson, N., 1982. Soil Conservation. Batsford Ltd., London.

Kallenbach, E.M.F., Rødland, E.S., Buenaventura, N.T., Hurley, R., 2022. Microplastics in terrestrial and freshwater environments. In: Bank, M.S. (Ed.), *Microplastic in the Environment: Pattern and Process*. Springer Nature, Cham, Switzerland, pp. 87–130.

Klein, M., Fischer, E.K., 2019. Microplastic abundance in atmospheric deposition within the Metropolitan area of Hamburg, Germany. *Sci. Total Environ.* 685, 96–103.

Kok, J.F., Parteli, E.J.R., Michaels, T.I., Karam, D.B., 2012. The physics of wind-blown sand and dust. *Rep. Prog. Phys.* 75, 106901.

Koohbanani, H., Barati, R., Yazdani, M., Sakhidari, S., Jomemanzari, R., 2018. Groundwater recharge by selection of suitable sites for underground dams using a GIS-based fuzzy approach in semi-arid regions. In: *Progress in River Engineering & Hydraulic Structures*. International Energy and Environment Foundation, pp. 11–32.

Koutnik, V.S., Leonard, J., Alkidim, S., DePrima, F.J., Ravi, S., Hoek, E.M.V., Mohanty, S. K., 2021. Distribution of microplastics in soil and freshwater environments: global analysis and framework for transport modeling. *Environ. Pollut.* 274, 116552.

Kuntze, H., Beinhauer, R., Tetzlaff, G., 1990. Quantification of Soil Erosion by Wind, I. Final Report of the BMFT Project. University of Hannover (in German).

Mendez, M.J., Funk, R., Buschazzo, D.E., 2011. Field wind erosion measurements with big spring number eight (BSNE) and modified Wilson and cook (MWAC) samplers. *Geomorphology* 129, 43–48.

Namikas, S.L., 2003. Field measurement and numerical modelling of aeolian mass flux distributions on a sandy beach. *Sedimentology* 50, 303–326.

Ravi, S., Li, J., Meng, Z., Zhang, J., Mohanty, S., 2020. Generation, resuspension, and transport of particulate matter from biochar-amended soils: a potential health risk. *GeoHealth* 4, e2020GH000311.

Rezaei, M., Riksen, M.J.P.N., Sirjani, E., Sameni, A., Geissen, V., 2019. Wind erosion as a driver for transport of light density microplastics. *Sci. Total Environ.* 669, 273–281.

Rezaei, M., Abbasi, S., Pourmahmood, H., Oleszczuk, P., Ritsema, C., Turner, A., 2022. Microplastics in agricultural soils from a semi-arid region and their transport by wind erosion. *Environ. Res.* 212, 113213.

Sarbazai, M., Ownegh, M., Behbahani, A.M., Akbari, M., 2020. Evaluating and modeling temporal-spatial changes of land use in the expansion of desertification intensity in the arid regions of northeast Iran (Sarakhs). *Geography and Environmental Hazards* 34, 1–6.

Shao, Y., Lu, H., 2000. A simple expression for wind erosion threshold friction velocity. *J. Geophys. Res.* 105 (D17), 22437–22443.

Sterk, G., Raats, P.A.C., 1996. Comparison of models describing the vertical distribution of wind-eroded sediment. *Soil Sci. Soc. Am. J.* 60, 1914–1919.

Sterk, G., Parigiani, J., Cittadini, E., Peters, P., Scholberg, J., Peri, P., 2012. Aeolian sediment mass fluxes on a sandy soil in Central Patagonia. *Catena* 95, 112–123.

Tian, X., Yang, M., Guo, Z., Chang, C., Li, J., Guo, Z., Wang, R., Li, Q., Zou, X., 2022. Plastic mulch film induced soil microplastic enrichment and its impact on wind-blown sand and dust. *Sci. Total Environ.* 813, 152490.

Wang, X.H., Liu, K., Zhu, L.X., Li, C.J., Song, Z.Y., Li, D.J., 2021. Efficient transport of atmospheric microplastics onto the continent via the East Asian summer monsoon. *J. Hazard Mater.* 414, 125477.

Webb, N.P., Galloza, M.S., Zobeck, T.M., Herrick, J.E., 2016. Threshold wind velocity dynamics as a driver of aeolian sediment mass flux. *Aeolian Research* 20, 45–58.

Wilson, S.J., Cooke, R.U., 1980. Wind erosion. In: Kirkby, M.J., Morgan, R.P.C. (Eds.), *Soil Erosion*. John Wiley & Sons, Chichester, UK, pp. 217–251.

Xiong, X., Tappenbeck, T.H., Wu, C.X., Elser, J.J., 2022. Microplastics in Flathead Lake, a large oligotrophic mountain lake in the USA. *Environ. Pollut.* 306, 119445.

Zhang, Y., Gao, T., Kang, S., Sillanpaa, M., 2019. Importance of atmospheric transport for microplastics deposited in remote areas. *Environ. Pollut.* 24, 112953.

Zhou, Q., Tian, C., Luo, Y., 2017. Various forms and deposition fluxes of microplastics identified in the coastal urban atmosphere. *Chin. Sci. Bull.* 62, 3902–3909.